A novel method to detect and classify material defects in crystalline solids after energetic particle impact simulations

F. Javier Domínguez-Gutiérrez[a], U. von Toussaint[a]

[a]*Max-Planck Institute for Plasma Physics, Boltzmannstrasse 2, 85748 Garching, Germany.*

Abstract

We present a novel method to analyze the material defects after energetic particle irradiation by computing a rotation invariant descriptor vector for each atom of a given sample. This new method is easy to use, does not require extreme computational resources, and is independent of the sample material, primary knock on atoms (PKA), and temperature. We applied the method to molecular dynamics simulations of deuterated and pristine tungsten lattices using a PKA of 1 keV at different velocity directions with a temperature of 300K, which emulates a neutron bombardment process. The number of W atoms that are affected during the collision cascade are classified and quantified with the method by considering first the most common defects like the interstitial sites and void/vacancies, which allow us to find other classification defect types. Deuterated samples exhibit consistently more defects than pristine ones.

Keywords: Tungsten, MD simulations, descriptor vectors, PCA

1. Introduction

Plasma facing materials (PFMs) in the next generation of nuclear reactors are subjected to extreme conditions due to the direct plasma interaction [1]. The induced material damage has to be analyzed by the identification, classification, and quantification of the PFM defects. This is complicated by potentially unforeseen atomic configurations after irradiation [2, 3]. Tungsten is a primary candidate as PFM for a fusion device [4]. It is therefore of interest to investigate the effect of deuterium decoration of W on the defect formation [5, 6].

Material defects can be analyzed by voronoi tessellation and Wigner-Seitz cells to count common defects as vacancies and interstitials [7, 8], and by describing the topology of individual grains, bubbles, and cells in three-dimensional polycrystals [9]. However, non-standard and unexpected material defects need to be classified and quantified to provide an insight about the damage after a disruptive impact of high-energy particles from fusion reactions. For this reason, the International Atomic Energy Agency set out a competition [10] to detect material defects in different metals. In this paper, we present a novel method to identify, classify, and quantify material defects regardless of the sample composition and temperature, and impact energy. Our numerical procedure is able to identify new material defect types other than the common ones like interstitial sites and vacancies/voids. It is based on the Smooth Overlap of Atomic positions method [11, 12] (SOAP) to compute the descriptor vector of individual atoms of a given sample, which describes their particular physical environment. SOAP is implemented in the QUantum mechanics and Interatomic Potentials package (QUIP) [13] that is a collection of software tools with a variety of interatomic potentials and tight binding packages.

This paper is organized as follows: In section 2, we present the computational methods that are utilized in our research work, followed by a description of the preparation of the samples used to perform MD simulations of a deuterated and pristine W lattice for 1 keV of primary knock-on atoms. We also briefly describe QUIP and the computation of the reference descriptor vectors that define our crystal defects classification. The crystal defect quantification and further results are shown in the section 3. Finally, in section 4, we discuss our results and provide concluding remarks.

2. Theory

2.1. Descriptor vectors

An ideal tool for the identification of distortions in a crystalline sample should be sensitive to changes in a local environment, but at the same time insensitive to ”global” changes like rotation of the sample or permutations of atoms of the sample. In addition, it should allow for some kind of calibration (e.g. not counting thermal fluctuations as defects). Furthermore, the possibility of a probabilistic interpretation instead of a binary yes/no-response would be beneficial. Most of the suggested approaches so far fail in one or more of these aspects or can only be applied to specific kinds of defects. For example, just using the Cartesian coordinates of the neighboring atoms would result in a false positive identification of a changed environment under simple rotation. Similarly the use of a vector of nearest-neighbor distances (which are invariant under rotation) has deficiencies. Very different atomic configurations can result in the same vector [11].

In this section, we outline the approach to compute the reference descriptor vector based on the QUantum mechanics and

Inter-atomic Potentials package (QUIP) [13]. Descriptor vectors can be considered as a footprint of the local environment of an atom [11, 12].

2.2. Descriptor vector computation

The analysis of the defects of a given material structure is started by first computing the descriptor vectors (DVs) of each atom of the sample, which are representations of the atomic neighborhood. As has been shown in Ref. [11], the DVs are, as desired, invariant to rotation, reflection, translation, and permutation of atoms of the same species, but sensitive to small changes in the local atomic environment [11]. We compute the DVs, that represent the atomic neighborhood of an atom i, based on the following truncated Gaussian density function [11],

$$\rho^i(\vec{r}) = \sum_j^{\text{neigh.}} \exp\left(-\frac{|\vec{r} - \vec{r}^{\,ij}|^2}{2\sigma^2_{\text{atom}}}\right) f_{\text{cut}}\left(|\vec{r}^{\,ij}|\right), \quad (1)$$

$\vec{r}^{\,ij}$ is given by the difference vector between the atom positions i and j. σ^2_{atom} denotes the broadening of the instantaneous atomic position, this parameter is set according to the lattice constant of the sample and takes into account the thermal motion. Finally, $f_{\text{cut}}\left(|\vec{r}^{\,ij}|\right)$ is a smooth cutoff function, which is required to limit the considered neighborhood of an atom. The kernel $\rho^i(\vec{r})$ can then be expressed in a basis set as obtained in [12] in terms of expansion coefficients, c_{nlm}:

$$\rho^i(\vec{r}) = \sum_{nlm}^{NLM} c^{(i)}_{nlm} g_n(r) Y_{lm}(\hat{r}), \quad (2)$$

here $c^{(i)}_{nlm}$ are the expansion coefficients that corresponds to the i-atom in the lattice, $g_n(r)$ is a set of orthonormal Gaussian radial basis functions, and $Y_{lm}(\hat{r})$ are the spherical harmonics. To achieve invariance against rotations of the local environment of atom i, Eq. 2 needs to be averaged over all possible rotations. Surprisingly, the final result has a simple form [12] , thus that the components of the normalized DV, q^i, are simply given by

$$\hat{q}^{\,i} = \left[\sum_m \left(c^i_{nlm}\right)^* c^i_{n'lm}\right]_{nn'l}, \quad (3)$$

where $\vec{q}^{\,i} = \hat{q}^{\,i}/|\hat{q}^{\,i}|$. We compute the DVs of the deuterated and pristine sample using the QUIP package with its python interface [13].

2.3. Calibration of the descriptor vectors

Using the sequence of Eq. 1 to 3 for each atom i of the sample a DV $\vec{q}^{\,i}$ can be computed. Depending on the choice of the expansion orders in Eq. 2 for the spherical harmonics and the radial basis functions the number of components of $\vec{q}$ varies. Here, we used $N = 4$, and $L = 4$ (with $-L \leq m \leq L$) which yields a DV with 51 $(0 \ldots 50)$ components (2). The difference between two local environments i and j can then be computed by the distance between the two corresponding DVs, $d = d\left(q^i, q^j\right)$. The distance measure is the standard euclidean distance $d^E = \sqrt{\sum_k \left(q^i_k - q^j_k\right)^2}$ which treats all vector components, k, identical or a weighted measure $d^M = \sqrt{\sum_k \left(\vec{q}^{\,i}_k - \vec{q}^{\,j}_k\right)^T \sum^{-1} \left(\vec{q}^{\,i}_k - \vec{q}^{\,j}_k\right)}$ i.e. the Mahalanobis distance measure [14]. To select an appropriate distance measure we used a MD simulation to generate a thermalized tungsten BCC-lattice at $T = 300$ K (see section 3), and computed the descriptor vector for all the atoms. This sample of DVs for a defect free but thermalized environment has been used to compute a mean reference vector $\langle\vec{y}\rangle$ for defect-free environments, as well as the variance and the covariance matrix $\sum^{-1} = \sum^{-1}(T)$. Following this, the distances of the thermalized environments from a perfect BCC-lattice without thermal fluctuations can be computed. This yields the coverage distance and variance of thermalized environments for a perfect lattice, and thus sets the scale for judging if a distortion of the local environments is present. For the computation of reference DVs for some other common types of defects a similar approach has been chosen: A small MD sample containing the defect (e.g. an interstitial) was prepared and the DVs of the atoms next to the defect were computed, subsequently acting as a fingerprint for this specific type of defect (see section 3).

2.4. Probability of being a lattice atom

The use of the Mahalanobis distance d^M allows a straightforward probabilistic interpretation of the distance. Given that the distance distribution d^M of a thermalized sample is close to a Gaussian distribution, then the probability, $P(\vec{q}^{\,i}|\langle y\rangle)$, of an atom i being in a locally undistorted lattice can be computed using

$$P(\vec{q}^{\,i}|\langle y\rangle) = P_0 \exp\left[-\frac{1}{2}\left(\vec{q}^{\,i} - \langle\vec{y}\rangle\right)^T \sum^{-1} \left(\vec{q}^{\,i} - \langle\vec{y}\rangle\right)\right], \quad (4)$$

where P_0 is the normalization factor and $\vec{q}^{\,i}$ is the DV of the atom i. For our present analysis we restrict the covariance matrix to be diagonal with the variances σ^2 as diagonal elements. This yields a quantitative measure for identifying/selecting defects, even for samples of different temperatures, where fixed criteria (e.g. maximum displacement) could easily fail.

2.5. MD simulations

The simulation box is initially prepared as a pristine single-crystalline W lattice cell with 48778 W atoms based on a BCC unit cell. The box has a dimension of $(28a, 28a, 28a)$ with $a = 0.316$ nm as the W lattice constant [15], for a sample temperature of 300K. Here, we chose room temperature because the majority of the experiments of tungsten damaging are done at this temperature [16, 17]. The deuterated W lattice is created by introducing 0.1 at % D (53 deuterium atoms) randomly distributed in the whole sample of tetrahedral interstitial positions. The samples are energy optimized and thermalized to 300 K, using a Langevin thermostat with a time constant of 100 fs [18, 19]. In Fig. 1, we show the prepared deuterated W lattice using the following color code: D atoms are represented as purple spheres; W atoms that are next to a D atom are displayed as green spheres; and lattice W atoms are shown as light-gray spheres to better visualize the deuterated sample.

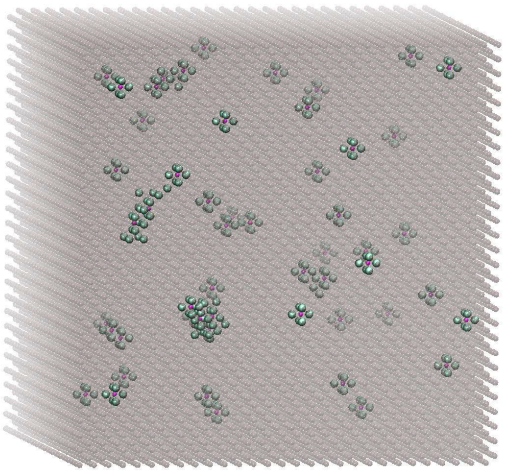

Figure 1: Deuterated W lattice. This lattice has been energy optimized and thermalized to 300 K. Colors: W atoms in a BCC position are presented as light gray spheres; W atoms around a D atom as depicted as green spheres; and D atoms are illustrated as purple small spheres.

MD simulations are performed by assigning an energy of 1 keV to a W atom, thus acting as a PKA. Its initial position is located at the center of the sample. We consider ten velocity directions: $\langle 001\rangle$, $\langle 011\rangle$, $\langle 111\rangle$, $\langle \frac{1}{2}0\frac{1}{2}\rangle$, and 6 cases for $\langle r_1 r_2 r_3\rangle$ where r_i are random numbers uniformly distributed in an interval of $[0, 1]$. A Velocity-Verlet integration algorithm is applied to model the collision dynamics, which lasts for 10 ps with a time step of $\Delta t = 1 \times 10^{-3}$ ps. After that time the dynamics of the collision cascade has stopped and the atom energies are thermalized. Subsequent diffusive relaxation process are thus missed, but their proper consideration would in any case exceed the time scale accessible for MD simulations. The simulations were performed on a desktop computer using the Large-scale Atomic/Molecular Massively Parallel Simulator (LAMMPS code) [20] with the reactive inter-atomic potential for the ternary system W-C-H of Juslin et al. [21], which is based on an analytical bond-order scheme. This MD potential has been used to study neutron damage in poly-crystalline tungsten [22], trapping and dissociation processes of H in tungsten vacancies [23], and cumulative bombardment of low energetic H atom of W samples for several crystal orientations [24].

3. Results

Initially, we computed reference DVs for the thermalized defect free BCC lattices for two temperatures, and two of the most common defects, interstitials atoms and W atoms next to single vacancy. For that, in order to compute the main reference vectors, we used a sample of 432 W atoms in a fully periodic box with a lateral dimension of ($5a$,$5a$,$5a$), based on a BCC unit cell of dimension $a = 0.316$ nm. A tungsten atom is removed from this sample to calculate the reference vector for atoms next to a vacancy. For the interstitial case, a W atom is introduced into the lattice at a tetrahedral interstitial site.

All the descriptor vectors are computed by QUIP with the SOAP descriptors package. We chose the following parameters: $l_{\max} = 4$, $n_{\max} = 4$, and a r_{ij} cutoff of 0.31 nm, slightly smaller than the unit cell of W, because of its lattice constant of 0.316 nm at 0K. A reference DV that takes into account thermal motion is calculated by a thermalized BCC sample at 300 and 600 K. These vectors are used to compute the probability of a W atom to be a defect in the W samples (Eq. 4), that are then classified. The computation of the reference DVs takes ~ 7 sec. for this particular size of the W sample on a desktop computer.

In Fig. 2, we show the amplitude of the reference DVs as a function of their components. The DVs for the W lattice at 0K (without thermal fluctuations) are shown in Fig. 2a). It can be seen that the structure of the non-zero components of the DVs for a tungsten atom in an ideal environment differs significantly from the structure of the DV of a W atom in a tetrahedral interstitial position. The non-zero pattern is almost identical for atoms next to vacancies compared to atoms in an undistorted lattice, nevertheless the different intensity-pattern allows an unambiguous assignment. These DVs for the lattice W atom, interstitial, and atom next to a vacancy, as well as their geometry are provided in the supplementary material. In Fig. 2b) and c) we present the DVs of all atom of the defect-free and thermalized BCC samples at 300 and 600 K, respectively. To provide a better visualization of the thermal descriptor vectors, we have used a bee-swarm plot: for component indices with intensities (> 0), the position is given by x+0.1x', where x' is a random number uniformly distributed in the interval $[-1, 1]$. Thus, the DVs for the W sample at 600 K have a bigger variance than those at 300 K. However, the mean of the components of the DVs at 300 and 600 K is very close to the components of

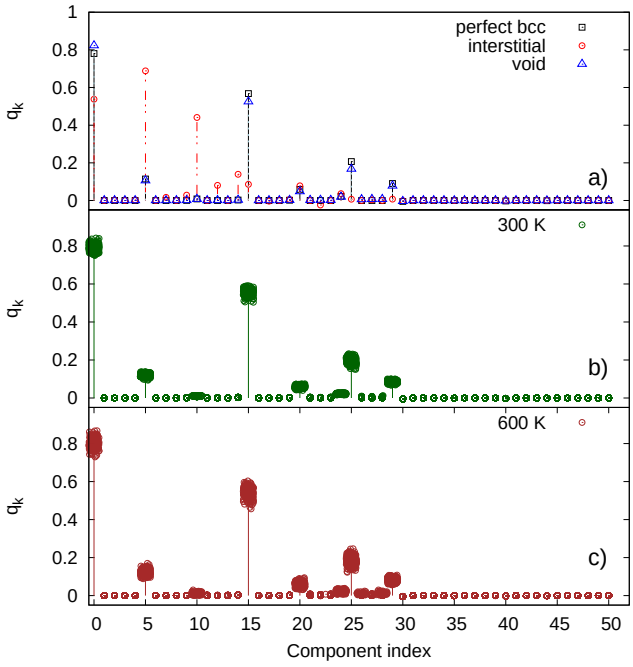

Figure 2: Amplitude of descriptor vectors as a function of their components. The main reference vector at 0 K is shown in a) and vectors of a defect free and thermalized W lattices at 300 and 600 K are presented in b) and c), respectively. These vector are used as reference descriptors to analyze the samples.

the lattice DV at 0K.

In Fig. 3a), we show the probability of an atom to be considered at a distorted site, i.e. $1 - P(q)$, as a function of the distance difference by using the DVs for a thermalized W sample to 300 (x-symbol) and 600 K (+-symbol) as a reference. Although, already the histogram of the distance from the DV for an atom of a BCC-lattice position of a thermalized tungsten lattice provides a good hint for a suitable distance value for the defects threshold, we followed another approach: a) By manual inspection of the local atom environment for different distance values it could be verified that the computed distance is indeed a good measure for the local disorder, i.e. exhibits a monotonic relation to the experts judgment and b) subsequently a suitable threshold can be selected by manual inspection of only a few configurations using bisection along the distance. In the inset graph, we note that only 0.07 % of the W atoms of the sample are eventually identified as defects. In Fig. 3b), we present a histogram of the distance difference between the DVs of the pristine W sample and the DV of the mean of the W lattice thermalized to 300 K ($\langle\vec{y}\rangle$), which is calculated by computing the difference between components as:

$$r_k^i = \frac{|q_k^i - y_k|}{\sigma_k}, \tag{5}$$

where q_k^i is the descriptor vector of the i-atom; y_k is the reference descriptor vector, for a thermalized sample this value is defined as the average of the amplitudes of each vector component; the k-index is the number of components of each vector; and σ_k is the amplitude variance of the DV the components.

Then, the distance difference, d^i, is obtained as

$$d^i = \left(\sum_k^N r_k^i \cdot r_k^i \right)^{\frac{1}{2}} \tag{6}$$

W atoms that have a distance greater than a threshold set at 0.15 are identified as defects. The identification of vacancies and interstitials is done by calculating the distance difference between the DVs of the sample and the reference DV of a W atom next to a vacancy and its interstitial site, respectively.

3.1. Defects classification of a pristine W sample

We classify and quantify the number of W atoms as interstitials, a W atom next to a vacancy, or other material defects by computing the distance difference between the DVs of the sample to each reference DV using Eq. 6.

In Fig. 4, we show the point defects of the pristine W sample, for a PKA velocity direction of ⟨001⟩. Only the actual sample defects are reported and the W atoms that are in a defect-free position are removed. Interstitials atoms in the W sample are represented by blue sphere, while W atoms next to a vacancy and type-a defects atoms are shown in red and green spheres, respectively. The interstitials sites are clustered on the path of the 1 keV PKA W atom. Vacancy sites and other defects are formed close to the trajectory path. A black W atom indicates the initial position of the projectile with its velocity direction displayed by a dashed line.

Using a principle component analysis of the obtained DVs (see sec. 3.2 for more details) revealed that besides interstitials and single vacancies a third type of a local defect structure was present, which was labeled as type-a defect. Subsequently, the structure of this type-a defect was elucidated by manual inspection of the involved atoms and verified by computing again the

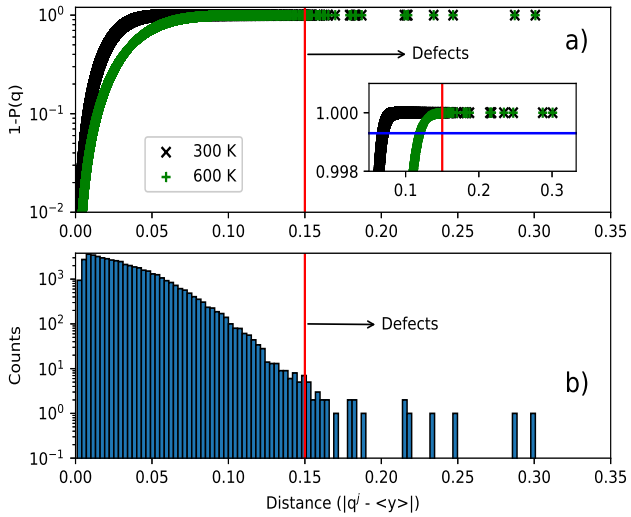

Figure 3: Probability of an atom to be identified as a defect of the W sample, as a function of the distance difference (Fig. 3a). Histogram of the results for the distance difference between the DV of the mean of the reference W lattice thermalized to 300K, with those for the W sample after 1keV collision cascade (Fig. 3b).

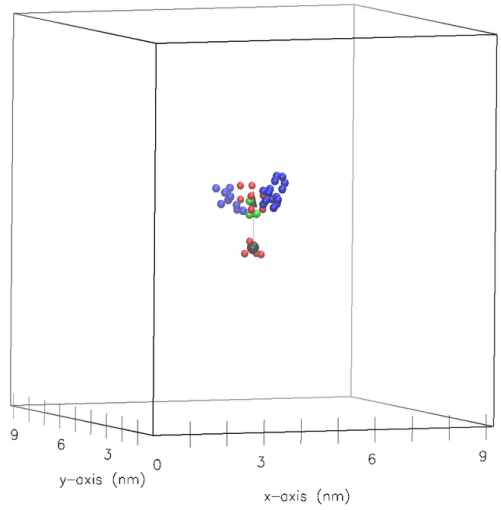

Figure 4: Defects of a pristine W sample at 1 keV with a velocity direction of ⟨001⟩. We include more W atoms next to a vacancy for a better visualization. The W atoms that are identified as defects are illustrated by sphere with the following color code: interstitial sites in blue; W atom next to a vacancy in red; type-a defect in green; and a W projectile in its initial position in black. Dashed arrow indicates the velocity direction of the projectile.

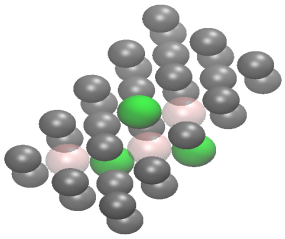

Figure 5: Atomic arrangement of the type-a defect (W atoms atom between two vacancies) found by PCA analysis of the descriptor vector of a pristine tungsten atom. Color code: type-a defect W atoms are represented by green sphere; gray and transparent pink spheres shown W lattice atoms and vacancies, respectively.

DV of the idealized structure. In Fig. 5 eight BCC unit cells are used to illustrate the atomic arrangement of the type-a W defect (green spheres), as a W atom between two vacancies (vacancies are represented by transparent pink spheres). We note that the W atom can be found either between two consecutive vacancies or just in the middle of the two vacancies. It is worth mentioning that the DV of a type-a W atom can be stored as a new reference vector and used in further analysis. In table 1, we list the total number of W atoms that are identified as an imperfect sites; the percentages of interstitial sites, W atoms next to a vacancy, and W atoms between two vacancies (type-a) for different velocity directions. In the same table, we report the average of the obtained results for the six MD simulations, that are performed for random velocity directions. The total number of defects for each velocity direction are: $\{34, 36, 33, 35, 31, 33\}$. The majority of the sample defects, found by our method, are interstitial sites and W atoms in the vicinity of them; while a minority of the defects is always observed as type-a. In the supplementary material, we provide a video to visualize the sample defects from different angles.

3.2. Defect classification of a deuterated W sample

The analysis of a multicomponent sample (here with W and D) can proceed by considering two approaches. In the first approach the reference DV for the tungsten atoms surrounding interstitial deuterium atoms are computed, while excluding the deuterium atoms from the computation. This allows to keep the computation of the descriptor vector identical to the monospecies case while accounting for the small displacements of the tungsten atoms induced by the interstitial deuterium atoms

Vel. dir.	**Inter.** (%)	**Vac.** (%)	**Type-a** (%)	**Total**
$\langle 001 \rangle$	72.7	21.2	6.1	33
$\langle 011 \rangle$	78.6	17.9	3.6	36
$\langle 111 \rangle$	69.7	21.2	9.1	35
$\langle \frac{1}{2} 0 \frac{1}{2} \rangle$	75.3	19.4	5.3	36
$\langle r_1 r_2 r_3 \rangle$	73.3	20.0	6.7	34
Average	73.9	19.9	6.2	35

Table 1: Defects quantification (in %) of a pristine W samples at different velocity directions. r_i with $i = 1, 2, 3$ are uniform random numbers in the interval $[0, 1]$.

and thus apparently allows to reuse all the descriptor vectors and thresholds of the W only case. Of course this approach will obviously fail for larger interstitial atoms because the atom displacements become too large, and it will become cumbersome for systems with more than two species. Unfortunately, the results of this first approach turn out to be not very convincing. A number of W atoms next to a vacancy are misclassified due to the removal of the D atoms from the sample. The results are reported in the upper half of the table 2 and one clearly sees the difference in the percentage of identified vacancies compared to the results of the second approach which is described below. Also the principal component analysis (PCA) of the DVs reveals that the they do not provide a good classification: the respective clusters are not clearly separated (cf. Fig. 6a). The results of the application of this first approach is given in Fig. 8a). Closer inspection shows that several W atoms which are next to a D atom have wrongly been identified as W atoms next to a vacancy.

Since the first approach does not provide viable results for the present case, the information about the D atoms needs to be included in the computation of a multi-component DVs for W atoms next to a D atom. This second approach is straightforward but increases the number of basis functions and also the required number of reference DVs. In Fig. 6b), we show the PCA results of the DVs of the deuterated W sample, where

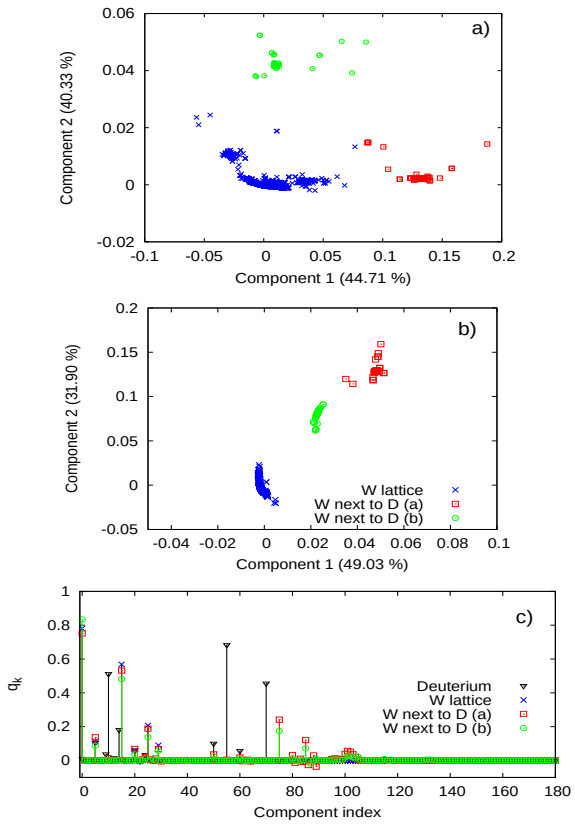

Figure 6: PCA results and DVs of the deuterated sample for the first approach in a) and for the second approach in b). The DVs are shown as a function of the component index for the second approach in c).

the first and second principal components capture 49.03 % and 31.90 % of the variance of the data. The cluster around the origin corresponds to the DVs of W lattice atoms in a defect-free environment. There are two clearly separated clusters with centers at the points (0.021, 0.08) and (0.055,0.13), that are associated to W atoms next to the D atom as first and second neighbors, respectively. Closer inspection reveal that W atoms that are next to an octahedral interstitial deuterium can be assigned the first-neighbor DV (a), and W atoms next to a tetrahedral D atom are identified by a second-neighbor DV (b).

In Fig. 6c), we show the DVs for a W atom lattice ($\times$ symbol); for a W atom next to a D atom, where (a) are first neighbors ($\square$) and (b) are considered as second neighbors ($\circ$) ; and for a D atom ($\triangledown$). Due to the inclusion of deuterium in the DVs computation, more components are needed. For our choice of parameters the descriptor vector for the two-component system has 180 components. We use these new DVs to identify those W atoms next to a D atom in the deuterated W sample, Fig. 1.

To analyze the deuterated W sample, let us first quantify the W atoms that are in interstitial sites. Following the approach described in the previous section, a distance difference histogram with respect to the reference DV for an interstitial tungsten atom is computed. In Fig. 7 we report the histogram of the distance difference between the chosen reference DV to the W atoms in deuterated sample in panel a) and compared to results for a pristine sample in panel b) to show the effect of the D atom in the formation of interstitials.

We summarize the number of defects in the deuterated W sample as a function of the PKA velocity direction in the Tab. 2, where the total number of defects for the individual random velocity directions are $\{35, 36, 36, 35, 31, 35\}$. Comparing the results of Sec. 3.1 (pristine W) with the present data for a sample with D, the results are revealing a small but persistent difference in the total number of defects between the two samples. In only

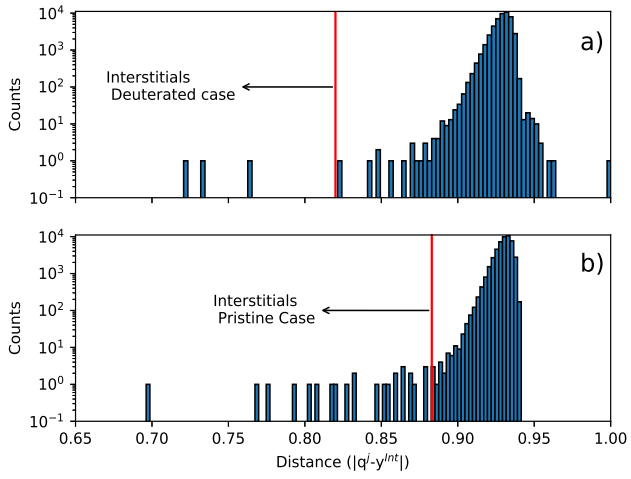

Figure 7: Histogram of the distance difference between the DV of a W in a interstitial site with those for the deuterated W sample in a), results for the pristine case in b) is included for comparison. The PKA direction for the considered sample is $\langle 001 \rangle$

Vel. dir.	**Inter.** (%)	**Vac.** (%)	**New type** (%)	**Total**
Approach 1				
$\langle 001 \rangle$	7.0	11.6	81.4	43
$\langle 011 \rangle$	6.8	11.4	81.8	44
$\langle 111 \rangle$	7.3	12.2	80.5	41
$\langle \frac{1}{2}0\frac{1}{2} \rangle$	6.5	10.9	82.6	46
$\langle r_1 r_2 r_3 \rangle$	6.6	11.1	82.3	45
Average	6.8	11.4	81.8	44
Approach 2				
$\langle 001 \rangle$	8.6	2.9	88.5	35
$\langle 011 \rangle$	8.1	2.7	89.2	37
$\langle 111 \rangle$	8.8	2.9	88.3	34
$\langle \frac{1}{2}0\frac{1}{2} \rangle$	7.7	2.6	89.7	39
$\langle r_1 r_2 r_3 \rangle$	8.6	2.9	88.5	35
Average	8.4	2.8	88.8	36

Table 2: Defect quantification (in %) of a deuterated W samples for different PKA velocity directions.

one out of all simulations the number of defects in the deuterated sample is smaller (by one count) than in the un-deuterated case and larger or equal in all other cases. Although the statistics is not very good, such a results should happen by chance in less than 2 % of all cases given that the defect probability is the same for both cases.

In Fig. 8b), we show the W atoms that are identified as defects in the sample for a PKA velocity direction of $\langle 001 \rangle$, where the spatial distribution of the defects is consistent with the results obtained for the pristine sample. Atoms identified as W lattice atoms and tungsten atoms next to a D atom are not shown for clarity. We provide an animation of this figure in the supplementary material. A black sphere is included in the figure to indicate the initial position of the projectile. D atoms are presented as small green spheres in the figure for a better visualization of the sample. W atoms colored in blue and red are identified as interstitials and vacancies, respectively. We conclude that the effect of Deuterium at the present level of concentration on the collision cascade is modest and the number of point defects defects is possible slightly larger compared to the pristine case.

4. Concluding Remarks

In this paper, we present a novel method to identify, classify, and quantify defects of a pristine and deuterated W sample after irradiation. We use QUIP to compute the descriptor vectors of all the atoms of the samples to describe the neighborhood of each atom. MD simulation are performed by LAMMPS with a PKA of 1 keV and a sample temperature of 300 K. We provide the descriptor vector for some of the most common cases like an atom in its body centered cubic location, an interstitial site, and an atom next to a vacancy, which have been used to analyze our samples after the collision cascade.

For the deuterated case, we use a principal component analysis to identify the descriptor vectors for a W atom next to a D atom, and for a D atom at a tetrahedral interstitial site. These

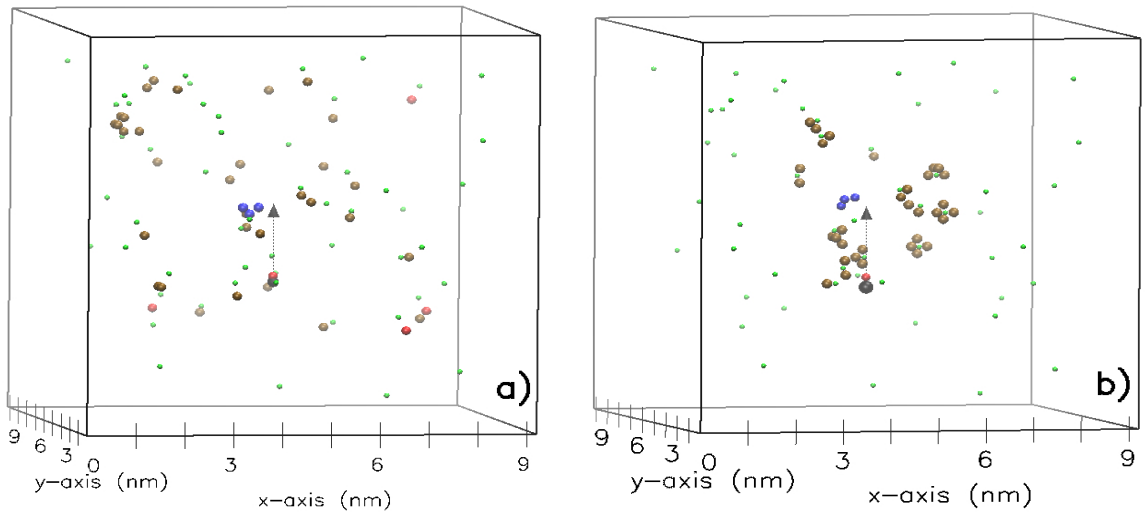

Figure 8: Defects of a deuterated W sample under the same conditions than the pristine one. W atoms are identified as possible sample defects by the computed DV of the first approach in a) and for the second approach in b). Color code: Interstitials are represented by blue spheres; W atoms next to vacancies are depicted in red spheres; a black sphere indicates the initial position of the projectile; W atoms that belong to a new type defect classification are illustrated as chrome spheres; and D atoms are resembled as small green spheres.

descriptor vectors are used to identify and quantify material defects for the W-D samples. Please note that the deuterated sample exhibits, with high probability, more defects than a pristine material although improved statistics is needed to substantiate this claim further. Future work is dedicated to analyze the effect of the impact energy and D concentration in the W sample on the creation of material defects, as well as the identification of new types of defects.

Acknowledgments

F.J.D.G gratefully acknowledges funding from A. von Humboldt Foundation and C. F. von Siemens Foundation for research fellowship.

Appendix A. Supplementary material

DVs and visualization videos

References

[1] J. Alvarez, A. Rivera, R. Gonzalez-Arrabal, D. Garoz, E. del Rio, J. M. Perlado, Materials research for hiper laser fusion facilities: Chamber wall, structural material and final optics, Fusion Science and Technology 60 (2) (2011) 565–569.

[2] H. Bolt, V. Barabash, G. Federici, J. Linke, A. Loarte, J. Roth, K. Sato, Plasma facing and high heat flux materials needs for ITER and beyond, Journal of Nuclear Materials 307-311 (2002) 43 – 52.

[3] M. Mayer, M. Andrzejczuk, R. Dux, E. Fortuna-Zalesna, A. Hakola, S. Koivuranta, K. Krieger, K. J. Kurzydlowski, J. Likonen, G. Matern, Tungsten erosion and redeposition in the all-tungsten divertor of ASDEX upgrade, Physica Scripta T138 (2009) 014039.

[4] M. Kaufmann, R. Neu, Tungsten as first wall material in fusion devices, Fusion Engineering and Design 82 (5) (2007) 521 – 527.

[5] P. Piaggi, E. Bringa, R. Pasianot, N. Gordillo, M. Panizo-Laiz, J. del Ro, C. G. de Castro, R. Gonzalez-Arrabal, Hydrogen diffusion and trapping in nanocrystalline tungsten, Journal of Nuclear Materials 458 (2015) 233 – 239.

[6] Z. Chen, L. J. Kecskes, K. Zhu, Q. Wei, Atomistic simulations of the effect of embedded hydrogen and helium on the tensile properties of monocrystalline and nanocrystalline tungsten, Journal of Nuclear Materials 481 (2016) 190 – 200.

[7] A. Okabe, B. Boots, K. Sugihara, S. N. Chiu, Spatial tessellations: concepts and applications of Voronoi diagrams, John Wiley and Sons, Inc., New York, NY, 2000.

[8] Y.-N. Liu, T. Ahlgren, L. Bukonte, K. Nordlund, X. Shu, Y. Yu, X.-C. Li, G.-H. Lu, Mechanism of vacancy formation induced by hydrogen in tungsten, AIP Advances 3 (12) (2013) 122111.

[9] E. A. Lazar, J. K. Mason, R. D. MacPherson, D. J. Srolovitz, Complete topology of cells, grains, and bubbles in three-dimensional microstructures, Phys. Rev. Lett. 109 (2012) 095505.

[10] IAEA Challenge on materials for fusion, `https://challenge.iaea.org/challenges/2018-NA-Mat-Fusion`, accessed: March 18th, 2019.

[11] A. P. Bartók, R. Kondor, G. Csányi, On representing chemical environments, Phys. Rev. B 87 (2013) 184115.

[12] W. J. Szlachta, A. P. Bartók, G. Csányi, Accuracy and transferability of gaussian approximation potential models for tungsten, Phys. Rev. B 90 (2014) 104108.

[13] `http://libatoms.github.io/QUIP/` (2018).

[14] P. Mahalanobis, On tests and measures of group divergence I. theoretical formulae, J. and Proc. Asiat. Soc. of Bengal 26 (1930) 541.

[15] W. Setyawan, G. Nandipati, K. J. Roche, H. L. Heinisch, B. D. Wirth, R. J. Kurtz, Displacement cascades and defects annealing in tungsten, part I: Defect database from molecular dynamics simulations, Journal of Nuclear Materials 462 (2015) 329 – 337.

[16] G. M. Wright, M. Mayer, K. Ertl, G. de Saint-Aubin, J. Rapp, Hydrogenic retention in irradiated tungsten exposed to high-flux plasma, Nucl. Fusion 50 (2010) 075006.

[17] A. Herrmann, H. Greuner, N. Jaksic, M. Balder, A. Kallenbach, et al., Solid tungsten divertor-III for ASDEX Upgrade and contributions to ITER, Nucl. Fusion 55 (2015) 063015.

[18] T. Schneider, E. Stoll, Molecular-dynamics study of a three-dimensional one-component model for distortive phase transitions, Phys. Rev. B 17 (1978) 1302.

[19] F. Domínguez-Gutiérrez, P. Krstić, Sputtering of lithiated and oxidated carbon surfaces by low-energy deuterium irradiation, Journal of Nuclear Materials 492 (2017) 56 – 61.

[20] S. Plimpton, Fast parallel algorithms for short-range molecular dynamics, Journal of Computational Physics 117 (1) (1995) 1 – 19.

[21] N. Juslin, P. Erhart, P. Träskelin, J. Nord, K. O. E. Henriksson, K. Nord-

lund, E. Salonen, K. Albe, Analytical interatomic potential for modeling nonequilibrium processes in the W-C-H system, Journal of Applied Physics 98 (12) (2005) 123520.

[22] U. von Toussaint, S. Gori, A. Manhard, T. Höschen, C. Höschen, Molecular dynamics study of grain boundary diffusion of hydrogen in tungsten, Physica Scripta 2011 (T145) (2011) 014036.

[23] B. Fu, M. Qiu, J. Cui, M. Li, Q. Hou, The trapping and dissociation process of hydrogen in tungsten vacancy: A molecular dynamics study, Journal of Nuclear Materials 508 (2018) 278 – 285.

[24] B. Fu, M. Qiu, L. Zhai, A. Yang, Q. Hou, Molecular dynamics studies of low-energy atomic hydrogen cumulative bombardment on tungsten surface, Nuclear Instruments and Methods in Physics Research Section B: Beam Interactions with Materials and Atoms (In press).